

Effect of siderurgical aggregates on concrete exposed to saline environments

Tamayo ^{P.^a}, Rico ^{J.^b}, López-Gayarre ^{F.^c}, Fiol ^{F.^d}, Panzera ^{T.H.^e}, Thomas ^{C.^{a,*}}, thomasc@unican.es

^aLADICIM (Laboratory of Materials Science and Engineering), University of Cantabria. E.T.S. de Ingenieros de Caminos, Canales y Puertos, Av./Los Castros 44, Santander 39005, Spain

^bConstruction Engineering, Research and Project Development (INGECID S.L.), University of Cantabria. E.T.S. de Ingenieros de Caminos, Canales y Puertos, Av./Los Castros 44, Santander 39005, Spain

^cCampus de Gijón, Department of Construction and Manufacturing Engineering, University of Oviedo, Asturias 33203, Spain

^dDepartment of Construction, University of Burgos. EPS, Calle Villadiego s/n, Burgos, Spain

^eCentre for Innovation and Technology in Composite Materials (CITeC), Department of Mechanical Engineering, Federal University of São João del Rei – UFSJ, São João del Rei, Brazil

*Corresponding author.

Abstract

Using recovered waste to obtain high-performance structural concrete is possible and justified by the saving in natural resources and the avoidance of deposit in landfills. The technical justification for these new and ecological concretes must be based on proving their mechanical performance and durability. The former has been widely studied, while the latter has been very vaguely studied, with controversies being found in this regard. This research aims to shed light on the ability of concrete with siderurgical aggregates to resist processes that lead to early deterioration or alteration of its microstructure. To this end, concrete with siderurgical aggregates and limestone reference concrete were subjected to traditional durability tests, as well as novel tests consisting of exposure to saline environments. The results obtained show that the concretes with siderurgical aggregates exhibit a similar behavior in terms of gas and water permeability, accelerated carbonation and resistance to freeze-thaw cycles (except for total replacements) to the limestone reference concrete. Exposure to a salt spray chamber and to seawater show the same effect in terms of chloride profiles, while the steel reinforcements embedded in the concrete did not suffer corrosion for any of the exposure times. These results open the door to using these concretes in maritime work, both onshore and offshore.

Keywords:

Siderurgical aggregates, Eco concrete, EAFS, Durability, Saline environments, Sustainability

Abbreviations

No keyword abbreviations are available

Data will be made available on request.

1 Introduction

Concrete is a construction material that consumes a large amount of raw materials and energy in its manufacture. To reduce the consumption of natural aggregates, which account for approximately 80 % by weight of conventional concrete, the research community has proposed different alternatives. Some examples include the use of recycled aggregates from construction and demolition waste (CDW) [1,2], from ballast and railway sleepers [3], or recovered steel slag aggregates [4–6]. The production of electric arc furnace slags (EAFS) in 2016 was 18 Mt in Europe [7] and much of this material ends up in landfill. The use of recovered EAFS provides siderurgical aggregates (SA) and their use in concrete constitutes not only a reduction in environmental impact but also an economic saving.

When replacing natural aggregate by SA, general improvements in the mechanical properties of concrete are obtained because the quality of the interfacial transition zone (ITZ) is superior [8] and because of the angular shape and rough texture of the SA [9]. Likewise, the use of SA as an aggregate for the manufacture of concretes implies a generalized increase in compressive strength [10–14], as long as the volume of cement paste remains constant, a property that makes them suitable for use in construction [15], providing high-strength concretes [16]. A greater replacement of natural aggregate by SA implies a higher compressive strength [17,18], whose values can increase slightly [19,20] or drastically, even reaching 150 % of the compressive strength of the reference concrete [5]. The elastic modulus is the property that increases the most, due to the high elastic modulus of the aggregates themselves [5,12].

The durability of these concretes is much less widely studied and seems highly dependent on the porosity and capillarity absorption of the concrete, since the voids and interconnected capillaries can facilitate the ingress of aggressive solutions [21,22]. Other important factors to take into account are humidity, temperature and fluid transport capacity [23]. There are positive studies such as the one carried out by Sideris [24] obtaining an improvement in the behavior of the concrete against carbonation and in residual strength after freeze-thaw cycles. This better behavior can be explained by the loss of aggregate-matrix adhesion being lower in the case of using SA [8]. Other authors, however, exclusively using SA as aggregate in the mixture, obtain a concrete with poorer behavior under freeze-thaw, showing a greater loss of mass [13], which is why they only recommend its use in warm areas where temperatures do not drop below 0 °C [25]. In this respect there is a controversy with the results obtained by another author [26], who found that the siderurgical aggregate mix is able to endure three times more freeze-thaw cycles than the reference mix. On the other hand, another author found that after freeze-thaw and wetting-drying tests, the comparisons between these SA mixes and other more conventional mixes have neither shown clear benefits nor excessively detrimental effects [27,28].

Regarding carbonation, it was found that the carbonation depth can be up to 6 times greater than that of a reference concrete with natural aggregates [28] or similar [26] depending on the study consulted. In a recent study, it was found that a self-compacting high-performance concrete with equally low permeability can be obtained with SA than with diabase aggregates. [29]. Moreover, there are studies where the use of SA slightly improves the durability of the concrete under exposure to chlorides in terms of reduction of the diffusion coefficient [30] and the depth of penetration of the chlorine ion when replacing the limestone fines by SA [24]. Some latest research work in the field of durability of concrete under saline environment includes the failed incorporation of fly ash in geopolymer concrete [1] or the improvement of chloride resistance using fly ash cenosphere (FAC) and sintered fly ash aggregate (SFA) in concrete [2]. Recent research has shown that the chloride penetrability decreases with BOF (coarse)/BOF (sand) ratio in aggregates replacement or fly ash/silica fume ratio in cementitious materials replacement [4]. Finally, progress has been made in the use of new materials for reinforcing bars, highlighting the recent implementation of FRP-concrete bonded reinforcement systems to minimize the effects of long-term exposure, economic costs and corrosion [3].

As has been shown, there is no tacit consensus about the, of concrete with SA compared to concrete that uses natural aggregates. This research aims to shed light on the potential durability of SA concrete. Three concrete mixes were designed for which the only variable to be modified was the type of aggregate to be used, keeping the volume of aggregates, amount of cement, w/c ratio, additive and effective water constant. The characterization carried out includes the physical properties of the concrete, permeability to gases and water under pressure, resistance to freeze-thaw cycles,


accelerated carbonation and specific tests consisting of exposure to saline environments. The latter include exposure to salt spray and immersion in seawater for different periods of time, allowing the level of corrosion damage in the reinforcements to be assessed. The results obtained will enable the suitability of these concretes to be established for structural application in maritime work, both onshore and offshore.

2 Materials and methods

2.1 Materials and mix proportions

For the manufacture of concrete, both natural aggregates (NA) and siderurgical aggregates (SA) were used. Limestone aggregates include fractions 12/18, 6/12 and 0/6 mm, while siderurgical aggregates (SA) include fractions 8/16, 4/8, 0/4 and 0/2 mm. The characterization of these aggregates includes the determination of the bulk density, apparent density and saturated-surface-dry density (SSD) in accordance with EN 1097-3 [31]. The porosity and water absorption were determined according to EN 1097-6 [32], the Los Angeles coefficient according to EN 1097-2 [33] and the aggregates crushing value (ACV) according to ISO 20290-3 [34]. Table 1 shows the results obtained, highlighting a similar water absorption and 30 % higher mechanical performance and density for the SA.

Table 1


 The table layout displayed in this section is not how it will appear in the final version. The representation below is solely purposed for providing corrections to the table. To preview the actual presentation of the table, please view the Proof.

Main properties of the aggregates used.

Aggregate	Bulk density [g/cm ³]	Apparent density [g/cm ³]	SSD density [g/cm ³]	Water absorption [% wt.]	Porosity [% vol.]	Los Angeles coeff. [%]	Aggregates crushing value [%]
NA	2.67	2.77	2.70	1.50	3.95	25	25
SA	3.83	4.04	3.88	1.44	6.52	17	18

The SA used come from a recovery process consisting of slow cooling (obtaining an amorphous structure) followed by inerting the periclase and lime by immersion in water. Finally, a crushing and screening operation of the aggregate is carried out to obtain different fractions. The chemical composition of SA largely depends on the composition and nature of the scrap used in the process (raw material) and the production processes involved in steel manufacture. Table 2 shows the oxide composition of the SA obtained by X-ray fluorescence (XRF) using an ARL-ADVANT-XP Thermo spectrometer.

Table 2

 The table layout displayed in this section is not how it will appear in the final version. The representation below is solely purposed for providing corrections to the table. To preview the actual presentation of the table, please view the Proof.

Composition in oxides of the SA used.

SiO ₂	Al ₂ O ₃	Fe ₂ O ₃	MnO	MgO	CaO	Na ₂ O	TiO ₂	P ₂ O ₅	SO ₃	V ₂ O ₅	Cr ₂ O ₃
10.57	6.19	44.79	5.95	7.09	21.99	0.03	0.51	0.29	0.27	0.36	5.53

The mix design was developed following the Fuller method [35] for a maximum aggregate size of 16 mm, setting a cement content of 340 kg/m³, the use of 1 % superplasticizer additive (SP) and an effective w/c of 0.47. The only variable that changed was the type of aggregate, maintaining the volume of aggregate used constant. Fig. 1(left) shows the proportions of the 3 designed mixes: limestone reference concrete (LLC), concrete with siderurgical aggregates and

limestone sand (SLC) and concrete with siderurgical aggregates only (SSC). The SSC mix incorporates sand crushed in the laboratory (SA 0/2) to make up for the lack of fines that SA commonly presents [36] and that in the SLC mix was compensated by adding NA 0/6 mm. Fig. 1(right) shows the grading of the set of aggregates used in each concrete mix.


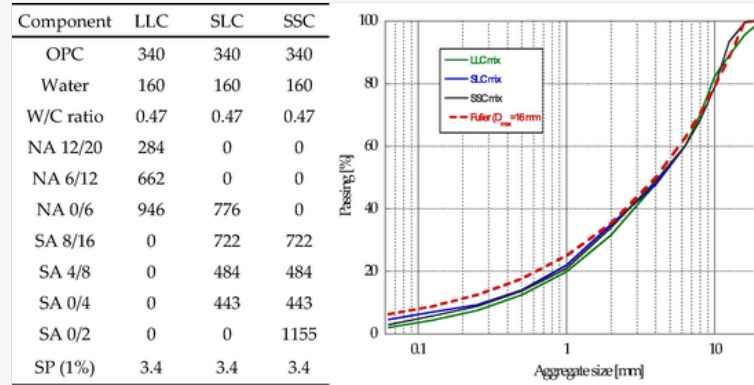
 Images are optimised for fast web viewing. Click on the image to view the original version.

Fig. 1



Mix proportions in kg/m³ (left) and grading of the designed mixes (right).

2.2 Physical properties of hardened concrete

The physical properties at 28 days were determined on six cylindrical specimens of 150x100 mm cut from standard cylindrical specimens (150x300 mm) for each mix. The bulk (D_b), apparent (D_a) and saturated-surface-dry (D_{ssd}) densities were determined, following the indications of the EN 12390-7 [37]. A vacuum pump was used to ensure the saturation of the specimens and additionally, the accessible porosity (% vol.) and the water absorption coefficient (% wt.) were determined in accordance with the formulations described in UNE 83,980 [38].

The ultrasonic pulse velocity (UPV) test was performed on five 100 mm cubes for each mix. Tests were carried out at 28 days of age with completely dry specimens, and the measurement were made according to EN 12504-4 [39]. The test was carried out using vaseline to ensure good acoustic coupling contact between concrete and transducer. A single transmitter and receiver were in direct transmission and the UPV was measured between the centres of the parallel lateral faces.

2.3 Permeability to gases and water

Oxygen permeability at 28 days was determined on six cylindrical specimens of 150x100 mm cut from standard cylindrical specimens (150x300 mm) for LLC and SLC mix. This property was obtained following the provisions of UNE 83,966 [40] and UNE 83,981 [41]. The specimens were completely dried in an oven at 110 ± 5 °C and coated with silicone on their lateral surface to ensure the sealing of the device. After penetrating the length of the test specimen, the outlet flow was determined for the test pressures of 1 and 2 bar, calculating the oxygen permeability (K_{O_2}) via the Darcy equation.

Water permeability at 28 days was determined on six cylindrical specimens of 150x100 mm cut from standard cylindrical specimens (150x300 mm) for the LLC and SLC mixes. The test was carried out as established by EN

12390-8 [42]. The test was performed maintaining a column of water at a pressure of 5 bar for 72 h. After this time, the specimens were broken using the Brazilian method (EN 12390-6 [43]) in a servo-hydraulic press with a capacity of 2500 kN, making it possible to observe the two fracture faces and measure the maximum depth of water penetration.

2.4 Freeze-thaw cycle resistance

Freeze-thaw cycle resistance was obtained on four 100 mm cubes for each mix, following EN-12390-9 [44], using the cube test (alternative method) and a deionized water solution. After 24 h of mixing, the test specimens were placed in a water bath at 20 ± 2 °C for 7 days and then kept at 20 ± 2 °C and 65 ± 5 % humidity (conditions that coincide with laboratory conditions) for 20 days.

The freezing and thawing pattern used in the test appears in Fig. 2, where the theoretical curve is the programmed curve, the chamber curve is the temperature inside the chamber and the interior temperature is the temperature measured inside one test specimen. Each cycle begins with a 16 h freezing phase (-18 °C for 2 h) for which an air-cooled chest freezer was used with an external tank where the water temperature is regulated. The thawing phase lasts 8 h and starts with the water rising inside the chamber until it reaches a height of 25 mm from the lid, leaving the containers in a bath (20 ± 2 °C for 4 h).


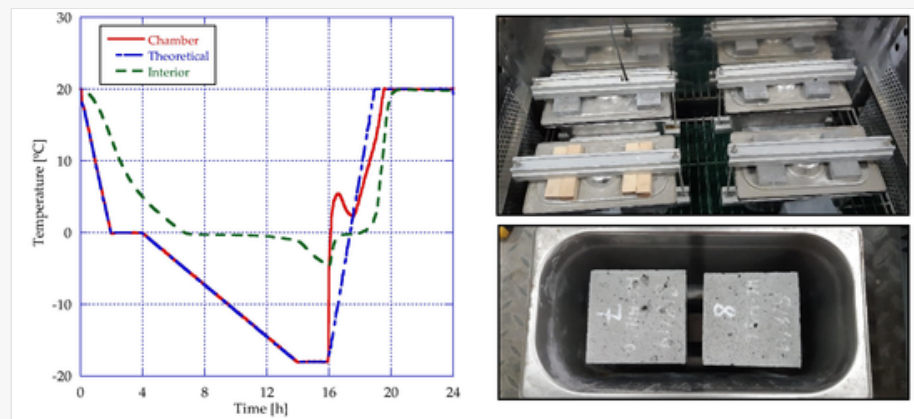
 Images are optimised for fast web viewing. Click on the image to view the original version.

Fig. 2



Recorded temperatures during a cycle and arrangement of containers inside the chamber.

After 7, 14, 28, 42 and 56 cycles the samples were brushed superficially and the dry weight of the detached material was recorded. After completing the test, the residual physical properties (EN 12390-7 [37] and UNE 83,980 [38]), the residual UPV (EN 12504-4 [39]) and the residual compressive strength (EN 12390-3 [45]) were obtained.

2.5 Carbonation resistance

Accelerated carbonation of the mixes LLC and SLC was determined on two cylindrical specimens (100x200 mm) per mix and age (28 and 91 days) for a total of 8 specimens. The specimens were subjected to standardized preconditioning (UNE 83,966 [40]), which consists of drying the specimens at 40 °C for 7 days and eliminating the drying gradients for 21 days sealed (with plastic wrap in this case) at 20 °C.

The carbonation process was carried out according to EN-83993-2 [46]: Accelerated method. The process was carried out in a chamber with controlled temperatures and humidity of 20 ± 2 °C and 65 ± 5 % respectively; the chamber environment having 3 % CO₂.

Finally, the resistance to carbonation was determined using the phenolphthalein method on the specimens that were subjected to accelerated carbonation. The phenolphthalein method is described in EN 14,630 [47] and a solution of 1 % by weight of phenolphthalein in ethanol was used. The depth of carbonation is measured as the distance between the

outer surface of the concrete and the edge of the region that has changed color with the solution (also called the carbonation front).

2.6 Exposure to saline environments

The penetration of chlorine ions into the concrete was determined for the LLC and SLC mixes by exposing two standard cylindrical specimens (150x300 mm) and a frusto-conical specimen (measures of an Abrams cone) with an embedded steel bar to the sea for 60 and 220 days. The specimens were manufactured with a steel hook embedded in their upper face and were placed in Santander Bay (Fig. 3).


 Images are optimised for fast web viewing. Click on the image to view the original version.

Fig. 3



Detail of the specimens and placement in the Santander Bay (Spain).

The frusto-conical specimen was manufactured by filling an inverted Abrams cone with concrete, in which a corrugated bar with a diameter of 10 mm was placed in its generatrix to evaluate the state of corrosion after marine exposure (the embedded part and the external part).

After a period of 60 or 220 days, the specimens were first visually inspected, after indirect tensile strength test was carried out to assess their internal state. Samples were taken from the cross-section at three heights. With these subsamples, after drying at 110 ± 5 °C until constant weight, the penetration depth of the chloride ions was determined using the X-ray dispersive spectroscopy technique, carried out with a scanning electron microscope (SEM).

The accelerated corrosion test was also carried out in a saline mist chamber on cylindrical specimens (100x200 mm) of the LLC and SLC mixes. The methodology followed is that of the EN ISO 9227 standard [48]. A WEISS TECHNIK SSC-1000 salt spray chamber with a capacity of 1000 L was used, with the following test parameters:

- Deionized water with a conductivity of 0.5 μ S/cm.
- Pharmaceutical grade sodium chloride (99 % purity).
- Solution concentration: 5 % by weight of NaCl.
- Test temperature: 35 °C.
- Flow rate throughout the trial: 1.38 ml/h.
- pH of the solution collected at the end of the test: 7.2.
- Test duration: 500 h.

After 500 h of direct exposure, the specimens were dried in an oven at 110 ± 5 °C until reaching a constant weight. Subsequently, a visual analysis of the outer surface of the specimens was carried out and they were split diametrically into two halves, obtaining subsamples that were analyzed similarly to the marine exposure subsamples.

3 Results and discussions

3.1 Physical properties of hardened concrete

Fig. 4(left) shows the densities of the mixes together with their standard deviations. All mixes that are not limestone control concrete exceed 2600 kg/m^3 , which is the density above which concrete is conventionally considered to be high density [49]. The application of these high-density concretes is wide, with a great role in gravity seawalls, breakwater structures (or other marine and port work), counterweights in bridges, precast blocks, or in radiation shielding structures [50]. The densities for the SLC and SSC mixes are 30 % and 40 % higher than those of the reference concrete, respectively.


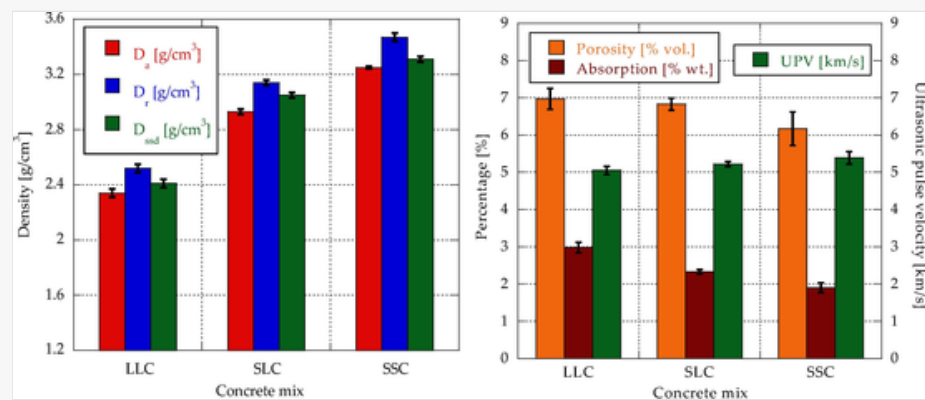
 Images are optimised for fast web viewing. Click on the image to view the original version.

Fig. 4



Physical properties of the mixes designed: densities (left) and porosity/absorption and UPV (right).

Fig. 4(right) shows the porosity and absorption of the mixes together with their standard deviations. The absorption decreases as the incorporation of SA does, this is because this property depends on the density of the concrete, so its comparison for concretes of different densities is not reliable. The porosity obtained is close to 7 % vol. in all cases, a low value [51] which shows the effectiveness of the vibration for the mixes that incorporate SA. Similar porosity is important when comparing the durability of concretes that incorporate different aggregates, since (a priori) the ability of aggressive external agents to pass through the pores will be similar.

Ultrasound pulse velocity (UPV) through concrete can define concrete durability since UPV is sensitive to cavities that concrete can contain. The UPV depends substantially on the porosity, the density and the elastic modulus of the concrete. The speed of the UPV decreases dramatically when it has to go through air, so the porosity of the paste (accessible and inaccessible), such as that of ITZ, as well as that of the aggregates themselves, and microcracks play a decisive role in this property. The concrete density is also important, since the ultrasound P-wave passes through compact structures with less difficulty.

Fig. 4(right) shows the UPV at 28 days for the four mixes manufactured, together with their standard deviations. Compared to the LLC mix, the SLC and SSC mixes show respectively 3 % and almost 5 % greater UPV. The increase is minimal but it is analogous to that shown by each of the concrete mixes in compressive strength in another work by the authors [50]. The UPV is related to compressive strength, since a structure with more internal voids slows down the UPV and also weakens the structural capacity of the concrete. Ultrasonic waves are also related to elastic modulus, since the vibrations introduced in the specimen are consistent with very small strains [52].

3.2 Permeability to gases and water

Gases can pass through concrete pores and discontinuities, such as micro-cracks, when they are subjected to high pressure. The oxygen permeability depends fundamentally on the interconnected porosity of the concrete, which allows the circulation of fluids and thus on the potential durability of the concrete. Another important factor is the humidity of

the atmosphere, which can fill part of the capillary pores and reduce air passage through them. It has been shown that an increase in relative humidity from 60 % to 95 % can reduce the permeability coefficient by two orders of magnitude [53]. This effect has been avoided by drying the specimens at 105 ± 5 °C before starting the test. The gas permeability coefficient decreases as the concrete becomes less permeable and can decrease by several orders of magnitude with increasing compressive strength [54].

Fig. 5 shows the oxygen permeability coefficient at 28 days for the LLC and SLC mixes with their respective standard deviations. The SLC mix shows a coefficient of permeability to oxygen 25 % higher than that of the LLC mix. However, the values obtained for both are extremely low (of the order of 10^{18}) and similar to those obtained by Sosa et al. [4] for high-performance self-compacting concrete with SA, showing good behavior against the penetration of gases.


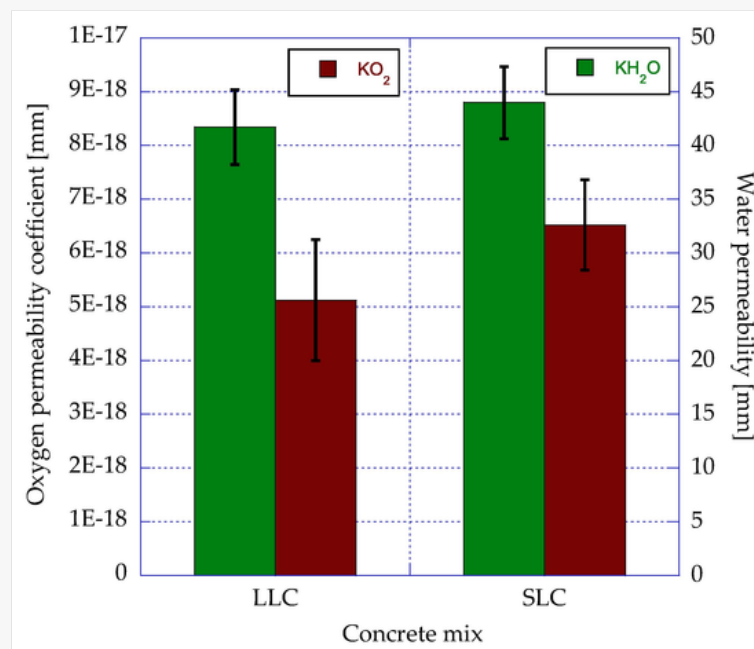
 Images are optimised for fast web viewing. Click on the image to view the original version.

Fig. 5



Permeability to oxygen and water under pressure.

The mechanism that governs oxygen permeability is the same as gas permeability, which is the permeation of fluid under pressure. Here the w/c ratio and the curing of the specimens play an important role, being mainly responsible for the existence of an interconnected network of pores. The difference concerning gases is that water needs a larger pore size to circulate. It is also important to emphasize the importance of aggregates because, although the cement paste is very impermeable, concrete may not be due to the porosity associated with ITZ or the scarcity of large aggregates (coarse).

Fig. 5 shows the permeability to water under pressure of the LLC and SLC mixes at 28 days, with their corresponding standard deviations. It can be observed that the SLC mix shows a maximum penetration 5 % greater than the LLC mix. In both cases, the values are below the 50 mm that the Spanish Structural Code [55] establishes as the limit.

3.3 Freezing-thawing cycles resistance

Freeze-thaw cycles can cause both internal damage and damage to the concrete surface. When the water in the concrete freezes, it expands, creating stresses. If these stresses exceed the tensile strength of the paste on the surface, breakage

occurs, leading to material peeling off the surface. There are conflicting ideas on improving the freeze-thaw resistance of concrete [56]. There is the idea of minimizing porosity (minimizing the w/c ratio) and thus the freezable water, but also the idea of employing an air-entraining agent. This latter idea is based on the fact that when entrained air bubbles (with a certain size and spacing) are introduced uniformly into the paste, pressure build-up is reduced [57]. Other factors that affect the durability under freeze-thaw cycles are the maximum and minimum temperatures, the number of cycles, size and geometry of the specimens, the type of cement, additives used (all kept constant) and the type of aggregates. All these factors except the type of aggregates and those that depend on the type of aggregates (such as porosity) were kept constant to assess the direct effect of each type of aggregate on durability.

Fig. 6, Fig. 7 and Fig. 8 show in detail the defects caused by passing cycles on the mixes LLC, SLC and SSC respectively. There is an enlargement of the pores on the surface of the specimens, with implications for the edges of the cubes and erosion of the faces of the cubes. The visualization reveals the character of this type of degradation, which is from the outside towards the inside of the concrete.


 Images are optimised for fast web viewing. Click on the image to view the original version.

Fig. 6



Appearance of LLC mix specimens after 56 cycles.


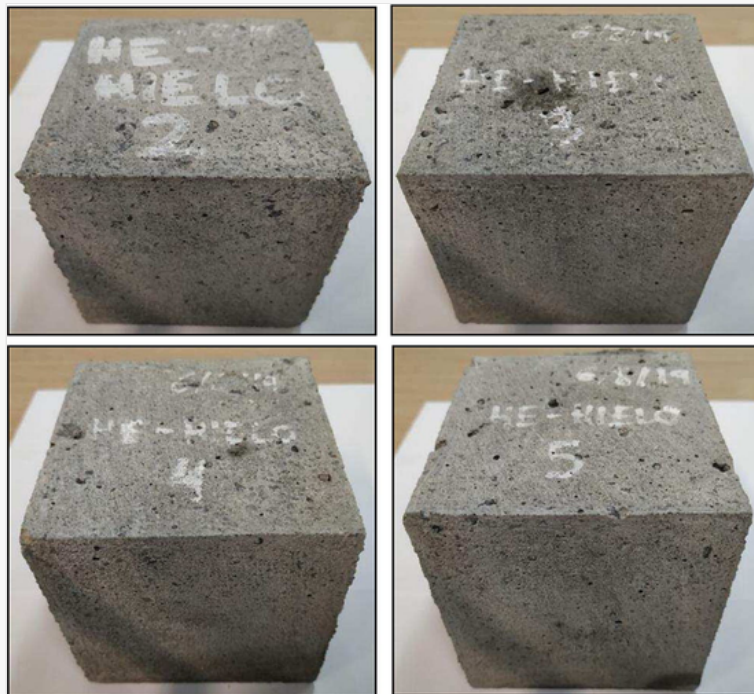
 Images are optimised for fast web viewing. Click on the image to view the original version.

Fig. 7



Appearance of SLC mix specimens after 56 cycles.


 Images are optimised for fast web viewing. Click on the image to view the original version.

Fig. 8



Appearance of SSC mix specimens after 56 cycles.

In addition to visual inspection, some physical properties have been characterized to quantify the level of degradation of the concrete. The main result of the test was the mass variation with the passage of cycles. Fig. 9(left) shows how the loss of relative mass of the specimens evolves. The days on which data were obtained correspond to 7, 14, 28, 42 and 56 cycles, as established by the standard. The evolution from cycle 14 is very similar for the 3 mixes, although there are differences during the first 7 and 14 cycles. At 7 cycles, the SSC mix has lost 5 times more material than the LLC mix, which corresponds to 60 % of the total material lost. The loss of mass of the LLC and SLC mixes is more progressive, although at 7 and 14 cycles, the LLC mix has lost twice as much mass as the SLC mix. As they are concrete mixes with very different densities, it is advisable to compare the evolution of the loss in volume of the released material. Fig. 9(right) shows this evolution: the behavior of the SSC mix becoming more similar to the LLC mix and the behavior of the LLC mix becoming more different from that of the SLC mix.


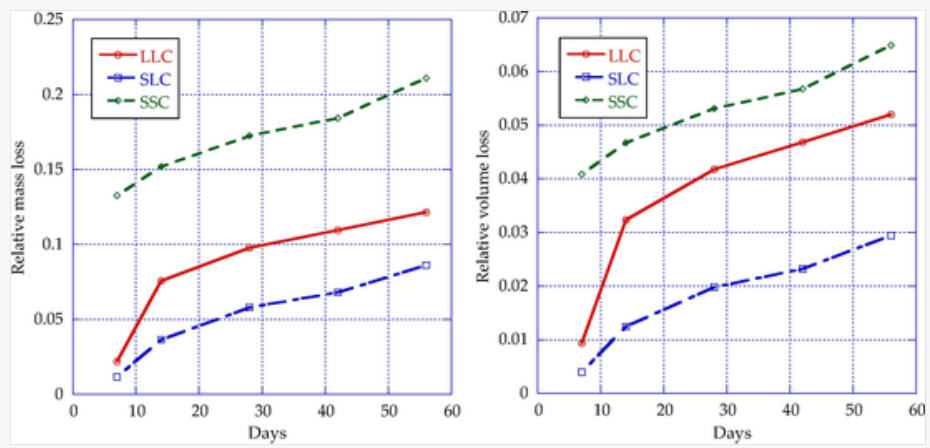
 Images are optimised for fast web viewing. Click on the image to view the original version.

Fig. 9



Relative mass loss (left) and volume loss (right) over cycles.

Table 3 shows the variation of porosity, absorption and mass, with their respective standard deviations. It can be observed that both the increase in porosity and water absorption is proportional to the incorporation of siderurgical aggregates. In contrast, this effect is not observed in the variation of mass. This may be because the siderurgical coarse aggregate adheres better to the cement paste, and although micro-cracks are generated (increased porosity), the aggregates do not detach (conservation of the mass).

Table 3

i The table layout displayed in this section is not how it will appear in the final version. The representation below is solely purposed for providing corrections to the table. To preview the actual presentation of the table, please view the Proof.

Variation of some physical properties after 56 cycles.

Mix	Porosity (% vol.)	Δ Porosity (%)	Absorption (% wt.)	Δ Absorption (%)	Δ mass (%)
LLC	8.84 ± 0.36	21.15	3.72 ± 0.16	19.89	-0.12
SLC	9.87 ± 0.16	30.80	3.45 ± 0.06	32.46	-0.09
SSC	9.73 ± 0.47	36.59	3.00 ± 0.16	36.67	-0.21

Furthermore, the residual compressive strength (Residual f_c) and the UPV after 56 cycles, with their respective standard deviations, were determined. Table 4 shows the results obtained. It can be observed that the increase in UPV (Δ UPV) describes the same behavior as the increase in porosity in Table 3. Surprisingly, this does not happen in the case of compressive strength for the SSC mix (it does for the other two), showing an a priori result incompatible with the variation of porosity or UPV. This may be because, in some way, the SSC mix specimens have kept the faces flatter, favoring the transmission of more homogeneous forces through them.

Table 4

i The table layout displayed in this section is not how it will appear in the final version. The representation below is solely purposed for providing corrections to the table. To preview the actual presentation of the table, please view the Proof.

Variation of f_c and UPV after 56 cycles.

Mix	Residual f_c (MPa)	Δf_c (%)	UPV (km/s)	Δ UPV (%)
LLC	44.93 ± 3.80	-28.58	4.94 ± 0.15	-2.26
SLC	59.04 ± 3.88	-34.00	4.82 ± 0.08	-7.70
SSC	59.04 ± 3.88	-34.00	4.82 ± 0.08	-7.70

SSC	84.17 ± 0.50	-23.76	4.72 ± 0.05	-12.47
-----	------------------	--------	-----------------	--------

3.4 Carbonation resistance

The parameters with most effect are the porosity of the concrete, the humidity of the environment and the exposure to rain, which reduce the amount of CO_2 that penetrates the concrete. Fig. 10 and Fig. 11 show the state of the specimens subjected to the accelerated carbonation process with an atmosphere of 3 % CO_2 , 20 ± 2 °C temperature and 65 ± 5 % relative humidity for 28 and 91-day exposures.


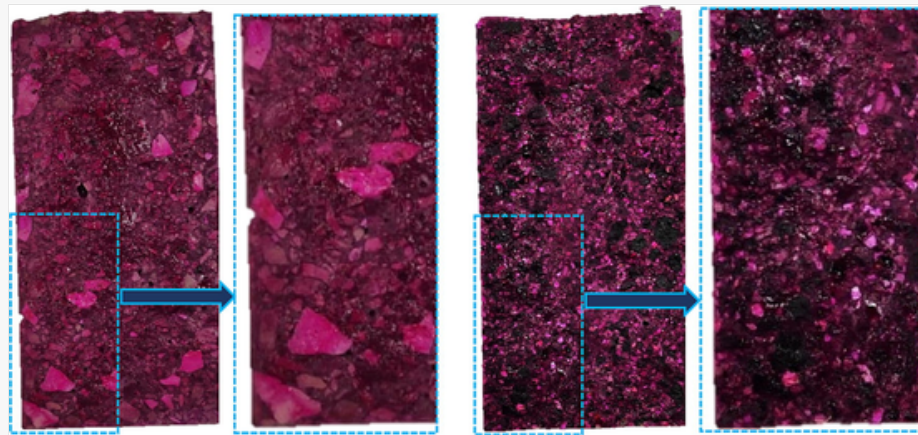
 Images are optimised for fast web viewing. Click on the image to view the original version.

Fig. 10



Appearance of mix LLC (left) and SLC (right) with an edge zoom at 28 days.


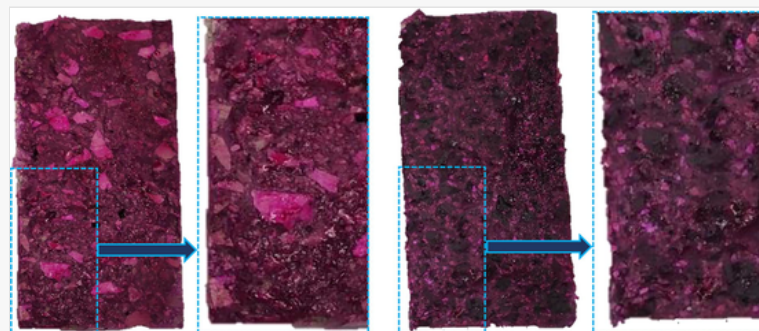
 Images are optimised for fast web viewing. Click on the image to view the original version.

Fig. 11



Appearance of mix LLC (left) and SLC (right) with an edge zoom at 91 days.

Each figure shows the sections of four different test specimens (two per mix) after applying the phenolphthalein solution. None of the eight test specimens tested, neither at 28 nor at 91 days, showed that the carbonation front had advanced from the surface to the interior of the specimens. The results show an excellent response to accelerated carbonation. Both mixes have a closed structure, very effective against the penetration of gases (as already analyzed in the gas permeability test) and aggressive atmospheres.

3.5 Exposure to saline environments

Initially, a visual analysis of the outer surface of the specimens exposed to salt spray (Fig. 12) was carried out, in which the accumulation of salt deposited on the surface can be observed, more noticeably in the lower part of the specimens. No type of degradation of the paste or corrosion of the siderurgical aggregate is observed. This can be verified in Fig. 11, where the generatrix of the specimens can be seen in a cross section, showing no degradation at the macroscopic level of either the paste or the aggregates or their interface. In addition, a clean break through the central section of the specimens was observed, without material being detached or finding traces of salt inside.


 Images are optimised for fast web viewing. Click on the image to view the original version.

Fig. 12



Visual appearance of the exterior and interior of the specimens exposed to salt spray.

A subsample was obtained from these specimens at 3 different heights of the specimen, extracted by hitting with a hammer perpendicular to the axis of the specimen. These subsamples were used to determine the concentration of chlorides with depth using SEM. The analysis under the SEM after the visual inspection enabled a chloride profile to be created, which showed how the Cl^- content varies with depth, considering this to be the perpendicular distance to the free surface of the concrete. Fig. 13 shows the concentration of the chlorine ion after exposure in the salt spray chamber for 500 h for the LLC and SLC concrete mixes. It can be seen that in both mixes the penetration capacity of the saline mist vapor depends on the depth of the specimen. The values obtained for both mixes can be considered very similar, with concentrations close to 1 % near the surface (the first reading was made at a depth of 0.2 mm). The concentration decrease with depth is in a negative exponential way. The fit obtained for both cases is acceptable in terms of the termination coefficient (R^2) but in no case is it excellent (it is not close to 1). The dispersion of the data obtained is due to the heterogeneous nature of the concrete itself, where the capillary network of the paste generates spaces that are more accessible to salt spray in certain places, especially in areas with the presence of macro-pores or where the surface finish was not perfectly smooth.


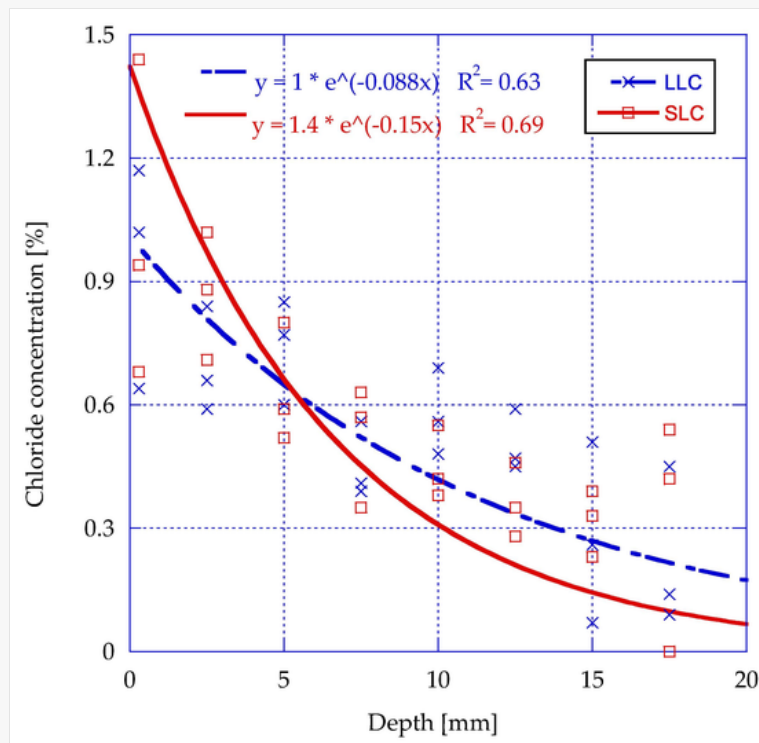
 Images are optimised for fast web viewing. Click on the image to view the original version.

Fig. 13



Chlorine ion concentration as a function of depth after exposure to salt spray.

Compared with the behavior after exposure to the marine environment, a certain similarity was observed with the concentration of chlorine ions after 220 days of exposure, although the exposure in the saline chamber seems to have involved a slightly more aggressive environment, perhaps because the fog is capable of percolating concrete more than seawater.

Exposure to seawater is one of the most common sources of chloride ions. The effect of chlorides in corrosion of concrete is very minimal; however, they can strip the protection layer of the reinforcements and corrode the steel, reducing the plastic strain of the reinforcing bars, especially if they are prestressed [54]. The transport mechanism of chlorides can be by diffusion or by capillarity through the network of pores, ITZ or cracks that the concrete may have. Therefore, both the water penetration and the porosity of the concrete will play an important role in determining the penetration of chlorine ions.

In the first place, a visual analysis of the state of the reinforcement of the reinforced concrete cone was carried out. This test was carried out with mixes LLC and SLC. Fig. 14 shows the appearance of the cone cut into two halves using a dry disc saw after 60-day exposure. Visible oxidation of the reinforcing bar can be seen in the sections that have not penetrated the concrete. At the same time, it maintains an unaltered state in the section where it is embedded in the concrete. On the other hand, oxidation was not reported in the siderurgical aggregate since iron is in the form of an oxide (mainly Fe_2O_3 and FeO) and not in the monoelemental form. Regarding the latter, steel flakes can be found in the siderurgical aggregate, their presence depending on the recovery capacity of the steel in the recovery process. A correct state of the paste and the concrete, in general, is also observed, which can be better appreciated in the enlarged images of the extremities in Fig. 14. Here the concrete near the surface and the outer concrete-rebar contact zone can be seen in detail, where an iron oxide film has formed.


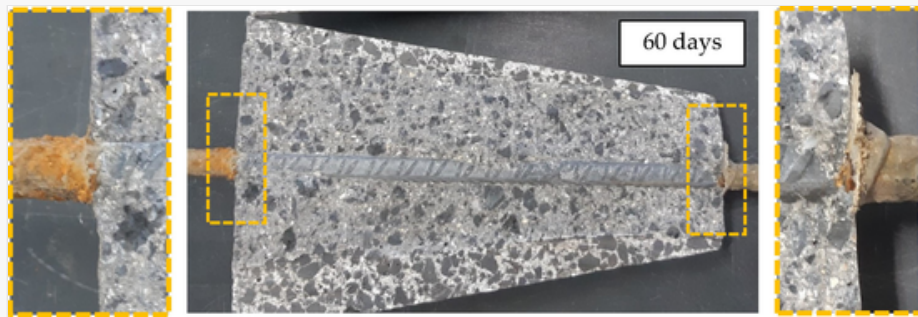
 Images are optimised for fast web viewing. Click on the image to view the original version.

Fig. 14



Appearance of the SLC mix and the rebar after 60 days of immersion.

Fig. 15 shows the longitudinal section of the reinforced truncated cone for a 220-day exposure to seawater. More advanced corrosion states can be observed in the bars not embedded in the concrete. Here the reinforcement has begun to chip on the surface, although it retains much of its structural integrity. The part embedded in the concrete shows no signs of pitting corrosion, having an intact state. On the other hand, the images still do not show corrosion in the aggregates. As in the case of exposure for 60 days, an iron oxide film is observed on the upper and lower surface of the frustocone around the reinforcement bar due to the detachment of oxide from the reinforcement and subsequent deposition. Finally, the enlarged images of the extremities in Fig. 15 show in detail the transition zone of the reinforcement within the concrete, verifying the perfect level of insulation of the embedded reinforcement.


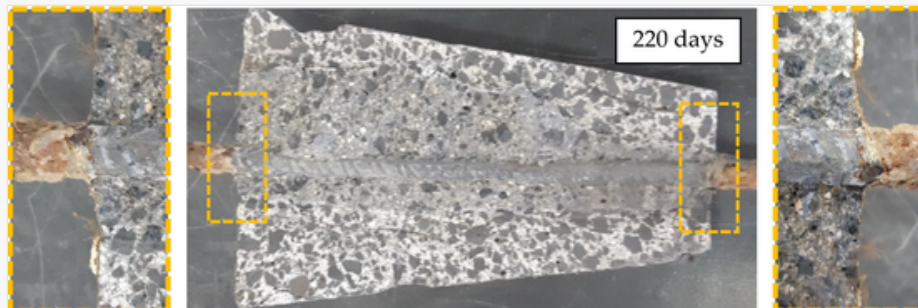
 Images are optimised for fast web viewing. Click on the image to view the original version.

Fig. 15



Appearance of the SLC mix and the reinforcing bar after 220 days of exposure.

EHE-08 and the Structural Code are strict regarding chloride ion content in concrete components. Both aggregates and cement must contain less than 0.05 % by mass of Cl^- for the manufacture of mass or reinforced concrete. This restriction increases to 0.03 % by mass for prestressed concrete. Portland cement meets these limits, while in siderurgical aggregates, chlorine was not detected in the X-ray fluorescence test (Table 1).

The effect of marine exposure on standard specimen cylinders was also analyzed to check the condition of the concrete after 60 days (Fig. 16).


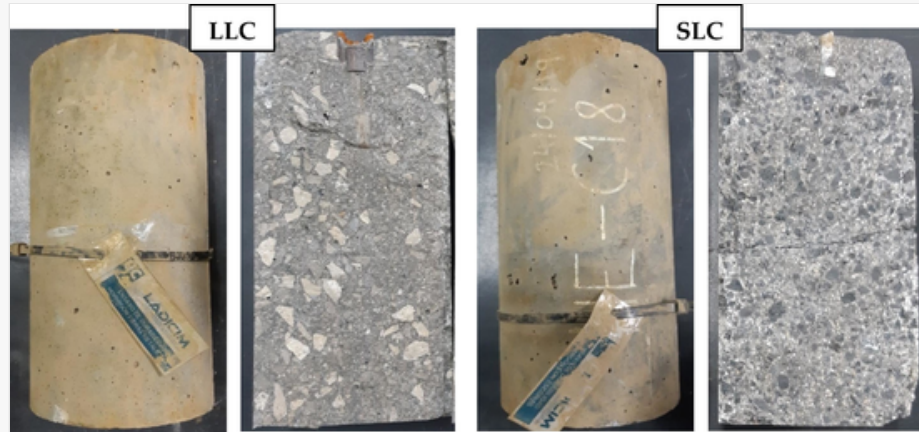
 Images are optimised for fast web viewing. Click on the image to view the original version.

Fig. 16



Visual appearance of the surface and the LLC and SLC mix after 60 days into seawater.

€As with the reinforced cones, no effect of seawater on the aggregates or the matrix was shown in any of the two mixes tested (LLC and SLC). The only visible effect was the external appearance of the specimen, which took on a greenish color due to the organic matter that had adhered to the surface.

After a period of 220 days, the second extraction of specimens exposed to the tidal race was carried out. The methodology developed was the same as with the 60-day test specimens. A longitudinal rupture of the specimen was performed using the Brazilian test (Fig. 17), and subsamples were taken at three different heights. The subsamples were dried and analyzed using an SEM.


 Images are optimised for fast web viewing. Click on the image to view the original version.

Fig. 17

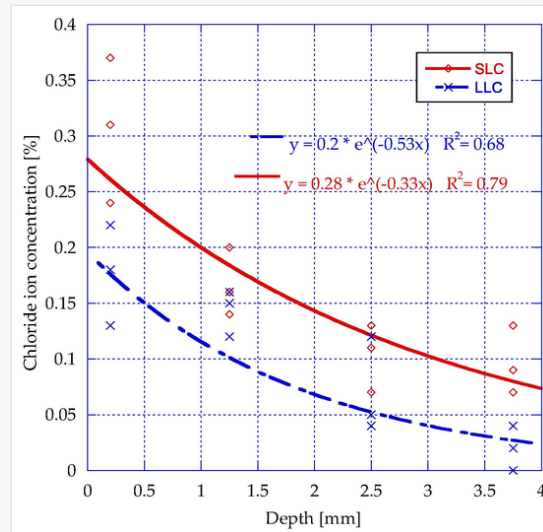


Visual appearance of the surface and the LLC and SLC mix after 220 days in seawater.

In this case, the test specimens showed an organic cover on their surface and even the presence of small mollusks for the specimens of both mixes (Fig. 17), but the sections of the test specimens, as for those with 60 days of exposure, did not show any sign of effect or degradation.

The SEM analysis after the visual inspection enabled a chloride profile to be created, which shows how the content of Cl^- varies with depth, considering this as the perpendicular distance to the free concrete surface. Fig. 18 shows the chlorine ion concentration after 28 days of curing and 60 days of marine exposure. Although it is a very short exposure time, the behavior that the mixes will have for greater ages can be revealed. The evolution of concentration with depth is similar to a negative exponential function, obtaining very low Cl^- even for areas very close to the surface. Although the values are very small, it can be observed that chlorine presence is approximately double in the LLC mix than it is in the SLC mix. As the concentrations are so extremely low, it can be concluded that concretes behave very well at such young ages.

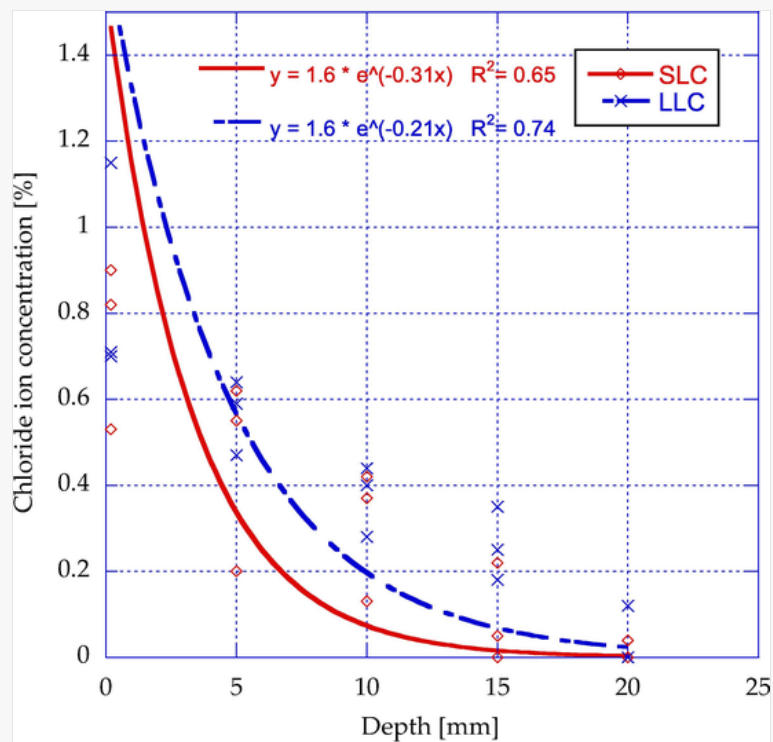
Fig. 18



Chloride penetration profile after 60 days of exposure.

Fig. 19 shows the chloride profile for the specimens of both mixes after 220 days of exposure to seawater. It can be seen that over the months, the entry of chlorides has increased notably; however, the trends of both mixes are very similar, although the SLC mix shows a slightly lower Cl^- content. The difference in densities between the two mixes (25 % higher in the case of the SLC mix) must also be taken into account since the results are expressed in % wt. of the sample. On the other hand, the results obtained at 220 days are compatible with the results obtained by Sosa et al., [58] in the control mixes after exposure to 10 months of tidal races.

Fig. 19



Chloride penetration profile after 220 days of exposure.

Regarding the limitations that appear in the regulations, EHE-08 limits the Cl^- content to 0.4 % of the weight of cement for mass or reinforced concrete and 0.2 % of the weight of cement for prestressed concrete. These limits are proposed for concrete in the state prior to its service, so they do not apply to concretes operating in aggressive environments. Thus, it can be seen that concentrations of 0.4 % are only reached for penetrations of less than 5 mm after 220 days of exposure.

4 Conclusions

In this research, the authors aimed to clarify the controversy that exists in the literature about the durability of concrete with siderurgical aggregates. The durability of concretes that incorporate siderurgical aggregates was analyzed, establishing their suitability by comparing the results with a limestone reference concrete. The tests carried out include physical properties, UPV, permeability to water and gases, accelerated carbonation, exposure to seawater and exposure to salt spray. After analyzing the results, the following conclusions can be drawn:

- The densities of the four mixes are coherent with the densities of the aggregates used, being 20 % – 30 % higher SA mixes. The porosity of all mixes was similar (about 7 % vol.), which indicates a similar durability under aggressive external agents and the UPV is slightly higher in denser mixes.
- The oxygen permeability coefficient is 25 % higher in the case of using SA, and the water absorption is similar for both mixes, indicating that indicates that the internal capillary network has a very small size.
- The response to accelerated carbonation was excellent for both the LLC mix and the SLC at both 28 and 91 days of exposure.

- After freezing-thawing cycles, the SLC mix lost less mass but showed greater porosity, UPV and compressive strength than the LLC mix. The SSC mix underwent greater degradation than the other two mixes.
- On exposure to salt spray, the Cl⁻ ion concentration for LLC and SLC mixes is very similar, with concentrations close to 1 % near the surface.
- Exposure to seawater after 60 and 220 days did not affect the reinforcement of the LLC mix or SLC mix specimens. Chloride ion penetration was low and similar in any case.

CRediT authorship contribution statement

Tamayo P. : Writing – review & editing, Writing – original draft, Visualization, Validation, Project administration, Formal analysis, Data curation, Conceptualization. **Rico J.** : Writing – original draft, Visualization, Validation, Supervision, Funding acquisition, Formal analysis, Conceptualization. **López-Gayarre F.** : Validation, Data curation. **Fiol F.** : Validation, Data curation. **Panzerä T.H.** : Writing – review & editing, Validation, Formal analysis. **Thomas C.** : Writing – review & editing, Writing – original draft, Visualization, Validation, Supervision, Project administration, Funding acquisition, Formal analysis, Conceptualization.


Declaration of Competing Interest

The authors declare that they have no known competing financial interests or personal relationships that could have appeared to influence the work reported in this paper.

Acknowledgments

This research was co-financed by the European Regional Development Fund (ERDF) and the Ministry of Economy, Industry and Competitiveness (MINECO) within the framework of the project RTC-2016-5637-3 and R&D project RES2020PU03 financed by the Department of Universities, Equality, Culture and Sports of the Government of Cantabria, Spain. The research was possible thanks to the collaboration of the company INGE CID, the department LADICIM (University of Cantabria) and the companies ROCACERO and SIDENOR, as well as the Department of Universities and Research, Environment and Social Policy of the Government of Cantabria (Spain).

References

 The corrections made in this section will be reviewed and approved by a journal production editor. The newly added/removed references and its citations will be reordered and rearranged by the production team.

- [1] P. Tamayo, J. Pacheco, C. Thomas, J. de Brito, J. Rico, Mechanical and Durability Properties of Concrete with Coarse Recycled Aggregate Produced with Electric Arc Furnace Slag Concrete, Appl. Sci. 10 (2020) 216.
- [2] C. Thomas, I. Sosa, J. Setién, J.A. Polanco, I. Lombillo, Mechanical behavior of recycled aggregates from concrete waste, WASTES Solut, Treat. Oppor. 1st Int. Conf. 1 (2011) 205–211.
- [3] J. Sainz-Aja, C. Thomas, J.A. Polanco, I. Carrascal, High-frequency fatigue testing of recycled aggregate concrete, Appl. Sci. 10 (1) (2020) 10.
- [4] I. Sosa, C. Thomas, J.A. Polanco, J. Setién, P. Tamayo, High Performance Self-Compacting Concrete with Electric Arc Furnace Slag Aggregate and Cupola Slag Powder, Appl. Sci. 10 (2020) 773.

[5]

S. Monosi, M.L. Ruello, D. Sani, Electric arc furnace slag as natural aggregate replacement in concrete production, *Cem. Concr. Compos.* 66 (2016) 66–72. [doi: doi: 10.1016/j.cemconcomp.2015.10.004](https://doi.org/10.1016/j.cemconcomp.2015.10.004).

- [6] G.G. Del Angel, A. Aghajanian, P. Tamayo, J. Rico, C. Thomas, Siderurgical Aggregate Cement-Treated Bases and Concrete Using Foundry Sand, *Appl. Sci.* 11 (2021) 435.
- [7] Euroslag, Statistics (2016, (2016).). <https://www.euroslag.com/research-library-downloads/download-s/>.
- [8] I. Arribas, I. Vegas, J.T. San-Jose, J.M. Manso, Durability studies on steelmaking slag concretes, *Mater. Des.* 63 (2014) 168–176.
- [9] F. Faleschini, A. Santamaria, M.A. Zanini, J.-T. San José, C. Pellegrino, Bond between steel reinforcement bars and Electric Arc Furnace slag concrete, *Mater. Struct.* 50 (2017) 170.
- [10] N.H. Roslan, M. Ismail, Z. Abdul-Majid, S. Ghoreishiamiri, B. Muhammad, Performance of steel slag and steel sludge in concrete, *Constr. Build. Mater.* 104 (2016) 16–24. [doi: doi: 10.1016/j.conbuildmat.2015.12.008](https://doi.org/10.1016/j.conbuildmat.2015.12.008).
- [11] P.O. Awoyera, A.W. Adekeye, O.E. Babalola, Influence of electric arc furnace (EAF) slag aggregate sizes on the workability and durability of concrete, *Int. J. Eng. Technol.* 7 (2015) 1049–1056.
- [12] M. Maslehuddin, A.M. Sharif, M. Shameem, M. Ibrahim, M.S. Barry, Comparison of properties of steel slag and crushed limestone aggregate concretes, *Constr. Build. Mater.* 17 (2) (2003) 105–112.
- [13] A.S. Brand, J.R. Roesler, Steel furnace slag aggregate expansion and hardened concrete properties, *Cem. Concr. Compos.* 60 (2015) 1–9. [doi: doi: 10.1016/j.cemconcomp.2015.04.006](https://doi.org/10.1016/j.cemconcomp.2015.04.006).
- [14] C. Pellegrino, P. Cavanis, F. Faleschini, K. Brunelli, Properties of concretes with Black/Oxidizing Electric Arc Furnace slag aggregate, *Cem. Concr. Compos.* 37 (2013) 232–240. [doi: doi: 10.1016/j.cemconcomp.2012.09.001](https://doi.org/10.1016/j.cemconcomp.2012.09.001).
- [15] L. Rondi, G. Bregoli, S. Sorlini, L. Cominoli, C. Collivignarelli, G. Plizzari, Concrete with EAF steel slag as aggregate: A comprehensive technical and environmental characterisation, *Compos. Part B Eng.* 90 (2016) 195–202. [doi: doi: 10.1016/j.compositesb.2015.12.022](https://doi.org/10.1016/j.compositesb.2015.12.022).
- [16] I. Papayianni, E. Anastasiou, Production of high-strength concrete using high volume of industrial by-products, *Constr. Build. Mater.* 24 (2010) 1412–1417. [doi: doi: 10.1016/j.conbuildmat.2010.01.016](https://doi.org/10.1016/j.conbuildmat.2010.01.016).
- [17] P.O. Awoyera, O.M. Olofinnade, A.A. Busari, I.I. Akinwumi, M. Oyefesobi, M. Ikemefuna, Performance of steel slag aggregate concrete with varied water-cement ratio, *J. Teknol.* 78 (2016) 125–131.
- [18] L. Coppola, A. Buoso, D. Coffetti, P. Kara, S. Lorenzi, Electric arc furnace granulated slag for sustainable concrete, *Constr. Build. Mater.* 123 (2016) 115–119. [doi: doi: 10.1016/j.conbuildmat.2016.06.142](https://doi.org/10.1016/j.conbuildmat.2016.06.142).
- [19] C. Pellegrino, V. Gaddo, Mechanical and durability characteristics of concrete containing EAF slag as aggregate, *Cem. Concr. Compos.* 31 (2009) 663–671. [doi: doi: 10.1016/j.cemconcomp.2009.05.006](https://doi.org/10.1016/j.cemconcomp.2009.05.006).
- [20] J.T. San-José, I. Vegas, I. Arribas, I. Marcos, The performance of steel-making slag concretes in the hardened state, *Mater. Des.* 60 (2014) 612–619. [doi: doi: 10.1016/j.matdes.2014.04.030](https://doi.org/10.1016/j.matdes.2014.04.030).

- [21] S. Assié, G. Escadeillas, V. Waller, Estimates of self-compacting concrete “potential” durability, *Constr. Build. Mater.* 21 (2007) 1909–1917, doi:10.1016/j.conbuildmat.2006.06.034.
- [22] C. Thomas, J. Setién, J.A. Polanco, J. de Brito, F. Fiol, Micro- and macro-porosity of dry- and saturated-state recycled aggregate concrete, *J. Clean. Prod.* 211 (2019) 932–940, doi:10.1016/j.jclepro.2018.11.243.
- [23] M. de F.-G. de España, EHE-08: Instrucción de Hormigón Estructural, (2008). http://www.fomento.gob.es/MFOM/LANG_CASTELLANO/ORGANOS_COLEGIADOS/CPH/instrucciones/EHE08INGLES/.
- [24] K.K. Sideris, A. Chatzopoulos, C. Tassos, Production of durable concretes using EAF slag aggregates, in: *Concr. Solut. – Proc. Concr. Solut. 6th Int. Conf. Concr. Repair*, 2016, 2016: pp. 625–630. <https://www.scopus.com/inward/record.uri?eid=2-s2.0-85015036391&partnerID=40&md5=db9f1453a34ed061f68054a227ca16f1>.
- [25] J.M. Manso, J.J. Gonzalez, J.A. Polanco, Electric arc furnace slag in concrete, *J. Mater. Civ. Eng.* 16 (2004) 639–645, doi:10.1061/(ASCE)0899-1561(2004)16:6(639).
- [26] I. Sosa, C. Thomas, J.A. Polanco, J. Setién, J.A. Sainz-Aja, P. Tamayo, Durability of high-performance self-compacted concrete using electric arc furnace slag aggregate and cupola slag powder, *Cem. Concr. Compos.* (2022). doi: doi: 10.1016/j.cemconcomp.2021.104399 104399.
- [27] A. Santamaría, A. Orbe, J.T. San José, J.J. González, A study on the durability of structural concrete incorporating electric steelmaking slags, *Constr. Build. Mater.* 161 (2018) 94–111. doi: doi: 10.1016/j.conbuildmat.2017.11.121.
- [28] M.A. González-Ortega, S.H.P. Cavalaro, G. Rodríguez de Sensale, A. Aguado, Durability of concrete with electric arc furnace slag aggregate, *Constr. Build. Mater.* 217 (2019) 543–556. doi: doi: 10.1016/j.conbuildmat.2019.05.082.
- [29] I. Sosa, P. Tamayo, J.A. Sainz-Aja, C. Thomas, J. Setién, J.A. Polanco, Durability aspects in self-compacting siderurgical aggregate concrete, *J. Build. Eng.* 39 (2021) 102268.
- [30] F. Faleschini, M.A. Fernández-Ruiz, M.A. Zanini, K. Brunelli, C. Pellegrino, E. Hernández-Montes, High performance concrete with electric arc furnace slag as aggregate: mechanical and durability properties, *Constr. Build. Mater.* 101 (2015) 113–121.
- [31] British Standards Institution, Tests for mechanical and physical properties of aggregates – Part 3: Determination of loose bulk density and voids, 1998.
- [32] EN 1097-6:2014, EN 1097-6 – Tests for mechanical and physical properties of aggregates – Part 6: Determination of particle density and water absorption, <Http://Www.Aenor.Es/>. (2014).
- [33] E.N. 1097-2:2010, Tests for mechanical and physical properties of aggregates. Methods for the determination of resistance to fragmentation, (n.d.).
- [34] International Organization for Standardization, ISO 20290-3: Aggregates for concrete — Test methods for mechanical and physical properties — Part 3: Determination of aggregate crushing value (ACV), (2019).

- [36] A. Sekaran, M. Palaniswamy, S. Balaraju, A study on suitability of EAF oxidizing slag in concrete: an eco-friendly and sustainable replacement for natural coarse aggregate, Sci. World J. 2015 (2015).
- [37] EN-12390-7, Testing hardened concrete – Part 7: Density of hardened concrete, (2009).
- [38] U.N.E. 83980:2014, Concrete durability. Test methods. Determination of the water absorption, density and accessible porosity for water in concrete., (2014).
- [39] E.N. 12504-4, Testing concrete – Part 4: Determination of ultrasonic pulse velocity, (2006).
- [40] U.N.E. 83966, Concrete durability. Test methods. Conditioning of concrete test pieces for the purpose of gas permeability and capilar suction tests., (2008).
- [41] U.N.E. 83981, Concrete durability. Test methods. Determination to gas permeability of hardened concrete., (2008).
- [42] E.N. 12390-8:2009, Testing hardened concrete – Part 8: Depth of penetration of water under pressure, (2009).
- [43] EN-12390-6, Testing hardened concrete – Part 6: Tensile splitting strength of test specimens, (2010).
- [44] C. 12390-9:2006, Testing hardened concrete – Part 9: Freeze-thaw resistance – Scaling, (2008).
- [45] E.N. 12390-3:2099/AC:2011, Testing hardened concrete – Part 3: Compressive strength of test specimens, (2011).
- [46] Part 1: Natural method. (2009).
- [47] EN 14630, Products and systems for the protection and repair of concrete structures. Test methods. Determination of carbonation Depth in Hardened concrete by the phenolphthalein method, (2007).
- [48] I.O. for Standardization, ISO 9227: Corrosion tests in artificial atmospheres – Salt spray tests, 2006.
- [49] B.S. 8500-2, Concrete-Complementary British Standard to BS EN 206-1. Part 2: Specification for Constituent Materials and Concrete, (2002).
- [50] P. Tamayo, C. Thomas, J. Rico, S. Pérez, A. Mañanes, Radiation shielding properties of siderurgical aggregate concrete, Constr. Build. Mater. 319 (2022) 126098.
- [51] J.A. Sosa, I. Tamayo, P.; Sainz-Aja, J.A.; Thomas, C.*; Setién, J. ; Polanco, I. Sosa, P. Tamayo, J.A. Sainz-Aja, C. Thomas, J. Setién, J.A. Polanco, Durability aspects in self-compacting siderurgical

aggregate concrete, J. Build. Eng. 39 (2021). doi: 10.1016/j.jobbe.2021.102268.

- [52] C. Thomas, J. Rico, P. Tamayo, F. Ballester, J. Setién, J.A. Polanco, Effect of elevated temperature on the mechanical properties and microstructure of heavy-weight magnetite concrete with steel fibers, *Cem. Concr. Compos.* 103 (2019) 80–88.
- [53] F. Tauscher, Einfluss des Wassergehalts auf die Gaspermeabilität von Mörtel und Beton, Shaker, 2005.
- [54] F.I. du Béton, Code-type models for structural behaviour of concrete, *fédération internationale du béton, Bulletin.* 70 (n.d.) 196.
- [55] M. de Fomento – Gobierno de España, Structural Code, (2019).
- [56] M.T. Bassuoni, M.L. Nehdi, The case for air-entrainment in high-performance concrete, *Proc. Inst. Civ. Eng. Build.* 158 (2005) 311–319.
- [57] H. Shang, W. Cao, B. Wang, Effect of fast freeze-thaw cycles on mechanical properties of ordinary-air-entrained concrete, *Sci. World J.* 2014 (2014).
- [58] I. Sosa, DOCTORAL THESIS: Incorporación de escorias siderurgicas en hormigones autocompactantes de altas prestaciones, 2017.

Highlights

- The porosity of the siderurgical aggregate concrete guaranty the durability.
 - Capillary network of siderurgical aggregate concrete is closed to fluids penetration.
 - No carbonation of siderurgical aggregate concrete is detected.
 - Exposure to seawater long periods did not affect the steel reinforcement.
-

Queries and Answers

Q1

Query: Please review the **given names and surnames** to make sure that we have identified them correctly and that they are presented in the desired order. Carefully verify the spelling of all authors' names as well. If changes are needed, please provide the edits in the author section. /

Answer: Reviewed

Q2

Query: Your article is being processed as a regular item to be included in a regular issue. Please confirm if this is correct or if your article should be published in a special issue using the responses below. /

Answer: Yes

Q3

Query: Correctly acknowledging the primary **fundors and grant IDs** of your research is important to ensure compliance with funder policies. Please make sure that funders are mentioned accordingly. /

Answer: Reviewed